Supporting Information

Optical Charge Trap Memory Based on Graphene/ZnO Heterostructures for Long-Term Retention and Adaptive Learning

Seungmin Shin†, Junhyung Kim†, Hyungdoh Lee, Yixuan Dou, Jacob T. Heiden, Seung Eun Lee, Jinwoo Song, Lina Quan, Giulia Tagliabue, Min Seok Jang, Himchan Cho**

S. Shin, H. Lee
Department of Materials Science and Engineering, Korea Advanced Institute of Science and Technology (KAIST), Daejeon, 34141, Republic of Korea

H. Cho*
Department of Materials Science and Engineering, Korea Advanced Institute of Science and Technology (KAIST), Daejeon, 34141, Republic of Korea
Graduate School of Semiconductor Technology, School of Electrical Engineering, Korea Advanced Institute of Science and Technology (KAIST), Daejeon, 34141, Republic of Korea
E-mail: himchan@kaist.ac.kr

J. Kim, J. T. Heiden, S.E. Lee, J. Song, M. S. Jang*
School of Electrical Engineering, Korea Advanced Institute of Science and Technology (KAIST), Daejeon, 34141, Republic of Korea
E-mail: jang.minseok@kaist.ac.kr

Y. Dou,
Department of Chemistry, Virginia Tech, Blacksburg, Virginia 24060, United States

L. Quan
Department of Chemistry, Virginia Tech, Blacksburg, Virginia 24060, United States
Department of Materials Science and Engineering, Blacksburg, Virginia 24060, United States

G. Tagliabue
Laboratory of Nanoscience for Energy Technologies (LNET), Ecole Polytechnique Federale de Lausanne (EPFL), Station 9, CH-1015, Lausanne, Switzerland

Figure S1.

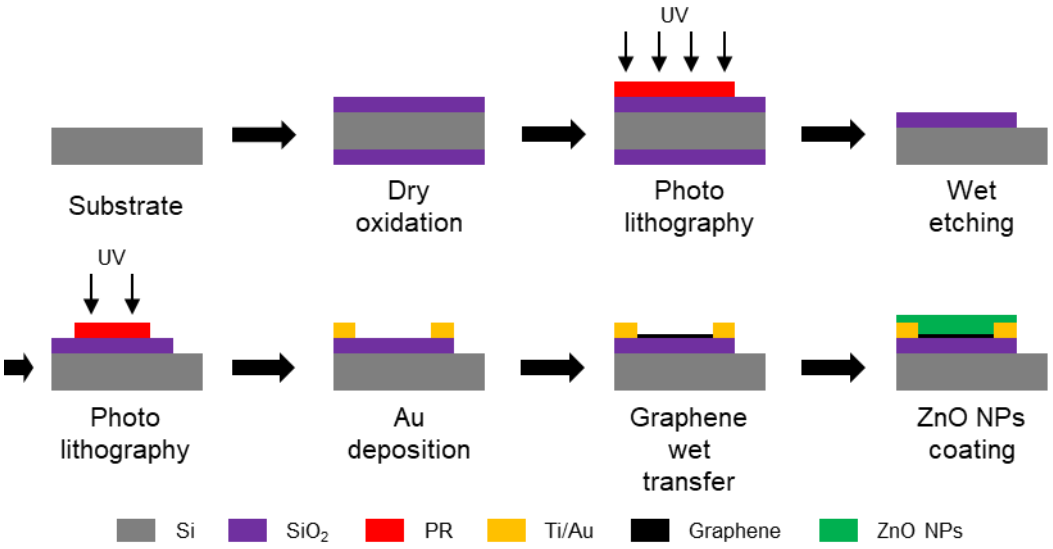

Figure S1. Device fabrication process of GZO optical CTMs.

Figure S2.

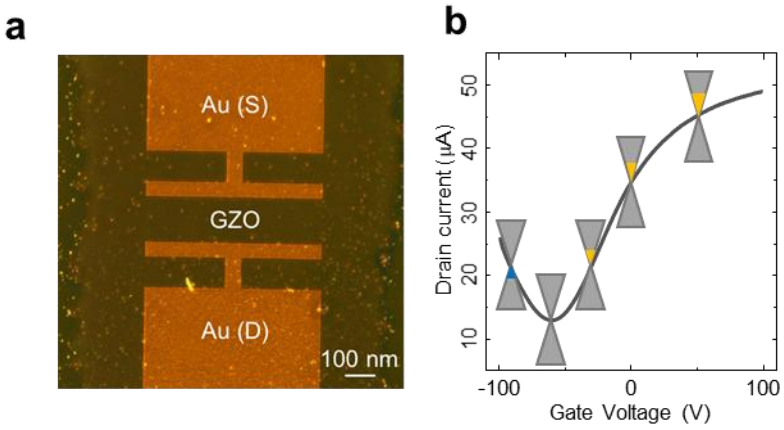

Figure S2. a. OM image of the GZO CTM device, **b**. Carrier concentration demonstration in I_d-V_g curve.

Figure S3.

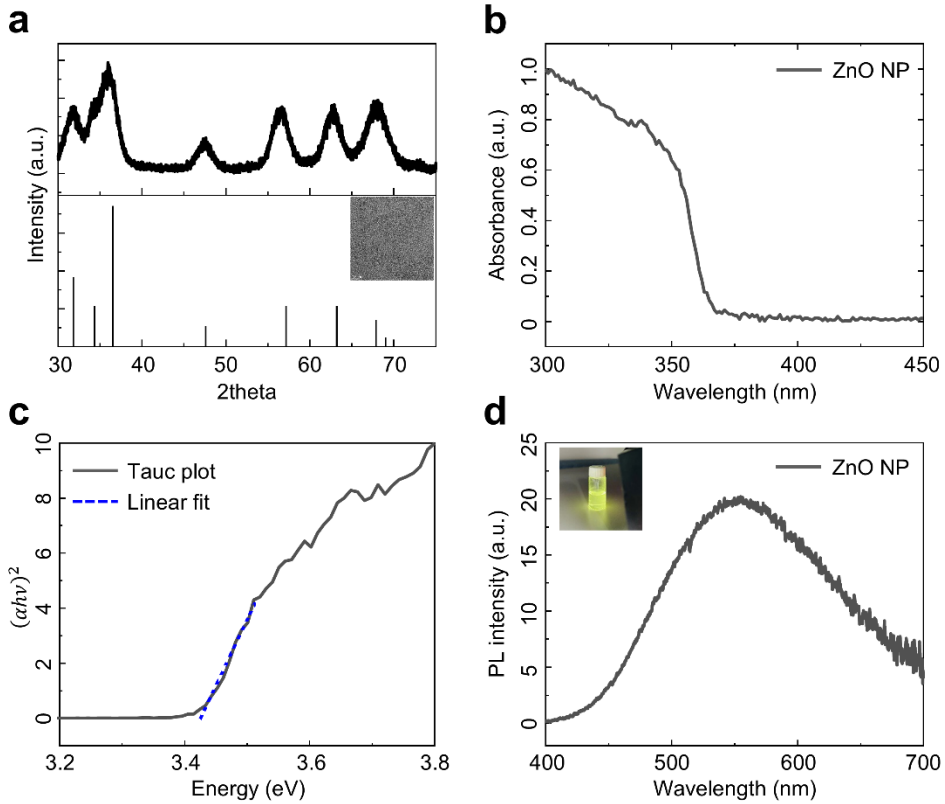

Figure S3. a. X-ray diffraction profile of ZnO absorbing layer spin-coated on Si substrate. The measured pattern is compared to simulated pattern based on the COD database (COD 1011258). **b.** Ultraviolet-visible light absorption of ZnO NPs. **c.** Calculated Tauc plot to obtain the optical band gap. **d.** Steady-state PL spectrum of ZnO NPs.

Figure S4.

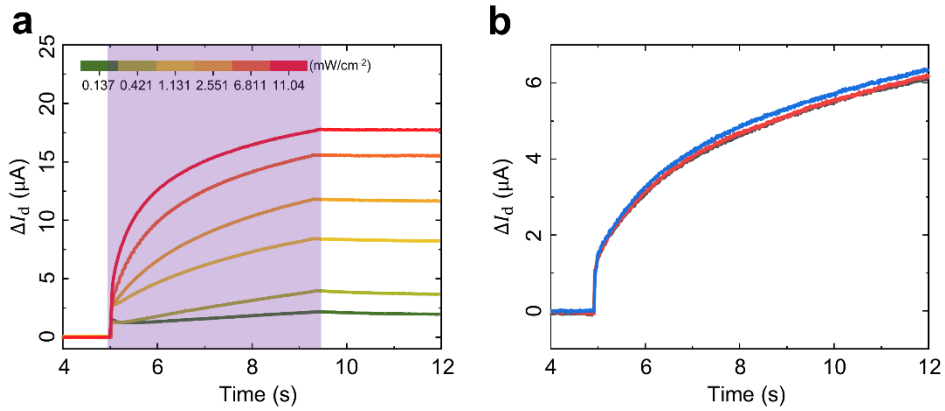

Figure S4. a. Highlighting increase region in Fig 1e**,** UV light was exposed with different power (purple box) **b.** Near unity increase slope with iterative UV light exposure (power 1.131 mW cm^{-2}).

Table S1. Exponential grow fitting of the increasing region in Figure S4

	y_0	A_1	t_1
0.137 mW/cm²	7.36772	-8.42877	22.7878
0.421 mW/cm²	10.5743	-16.5717	11.9662
1.131 mW/cm²	10.9201	-50.0192	3.65879
2.551 mW/cm²	13.7771	-122.251	2.68757
6.811 mW/cm²	16.6452	-310.94	1.98744
11.04 mW/cm²	18.4536	-369.58	1.83495

.

Figure S5.

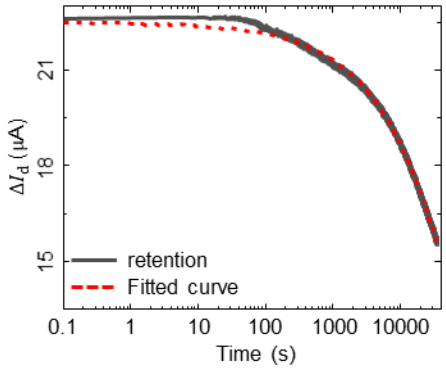

$$I = I_0 \exp\left[-\left(\frac{t}{\tau}\right)^{\beta}\right] + I_\infty$$

I_0 (μA)	β	τ (s)	I_∞ (μA)
27.14036	0.53197	345649.9	-4.64655

Figure S5. Retention time fitting by using Kohlrausch stretched exponential function.

Figure S6

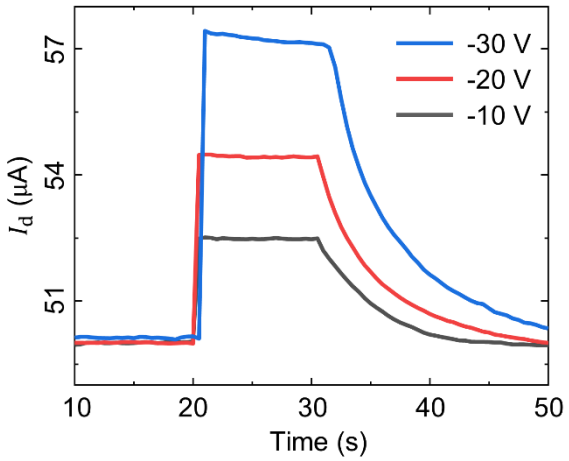

Figure S6. Retention with electrically doped carrier in GZO optical CTM

Figure S7

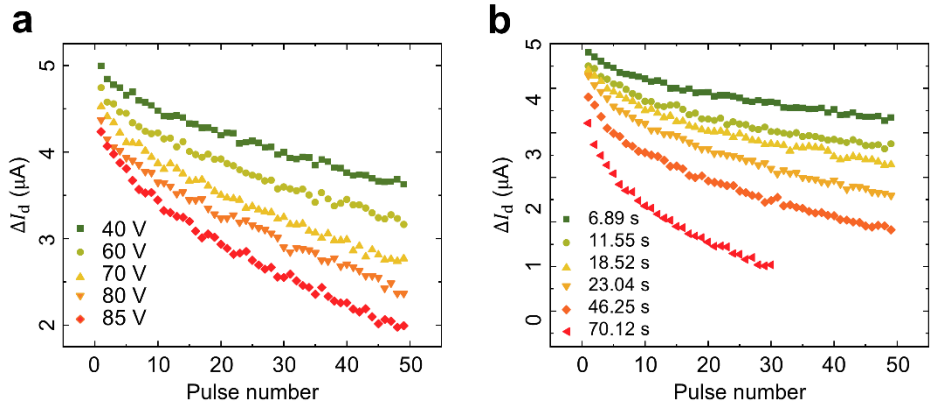

Figure S7. a. Current level recovery tendency as electrically gate bias increases (pulse period = 6.89 s), **b.** Current level recovery tendency as pulse period increases (gate bias = 60 V).

Figure S8

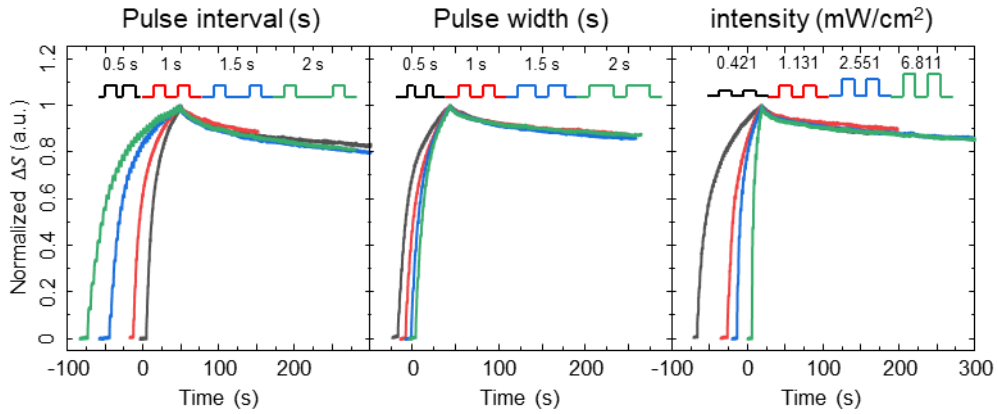

Figure S8. Retention decay behavior of the GZO CTM under varying light pulse conditions, including different intervals, pulse widths, and pulse intensities, respectively. The decay profile exhibits consistent trends across all conditions, indicating that the decay dynamics are mostly governed by the magnitude of conductance change rather than the specific pulse parameters.

Table S2. Comparison of previously reported optical charge trap memory devices.

Channel Materials	Light Source	Retention time	Learning simulation	type	ref
$CuIn_7Se_{11}$	543 nm	~ 50 s	-	Interface trapping	[1]
MoS_2	450 nm	~ 10,000 s	-	Interface trapping	[2]
Graphene/MoS_2 or WS_2	532 nm	~ 1,000 s	Winner-take-all model	Interface trapping	[3]
Graphene/$MoTe_2$	635 nm	> 86,400 s	Edge detection	Ferroelectric	[4]
Single wall carbon nanotube (SWCNT)/ Graphadiyne	405 nm ~ 1800 nm	> 10,000 s	ANN	Interface trapping	[5]
GaAs/P_3HT	261 nm ~ 1550 nm	> 100 s	Reservoir Computing	Interface trapping	[6]
SWCNT/PVP + Ag_2S	365 nm ~ 650 nm	~ 1,200 s	Bell response	Interface trapping	[7]
Pentacene/ PTCDI-C_{13}	400 nm ~ 700 nm	> 1,000 s	CNN based Image recognition	Interface trapping	[8]
Porphyrine/ZnO	365 nm ~ 625 nm	> 10,000 s	Visual perception	Interface trapping	[9]
$MAPbBr_3$/ZnO	365 nm, 532 nm	> 100 s	-	Interface trapping	[10]
Graphene/MoS_2	395 nm, 660 nm	> 200 s	-	Interface trapping	[11]
P_3HT/AlO_x	450 nm ~ 650 nm	> 100 *s*	Learning-Forgetting-Relearning	Interface trapping	[12]
Graphene/ZnO	365 nm	~ 195,790 *s*	ANN	Interface trapping	This Work

Figure S9

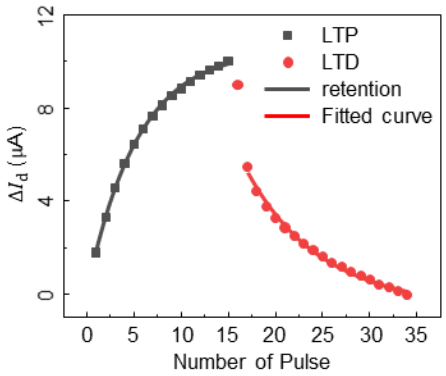

Positive update = $A_p(1 - \exp(-\frac{t}{\tau_p}))$

Negative update = $A_d \exp(-\frac{t}{\tau_d})$

A_p	τ_p	A_d	τ_d
10.50	5.43	50.81	7.81

Figure S9. Nonlinearity of positive update and negative update in GZO optical CTM for ANN simulation.

Figure S10

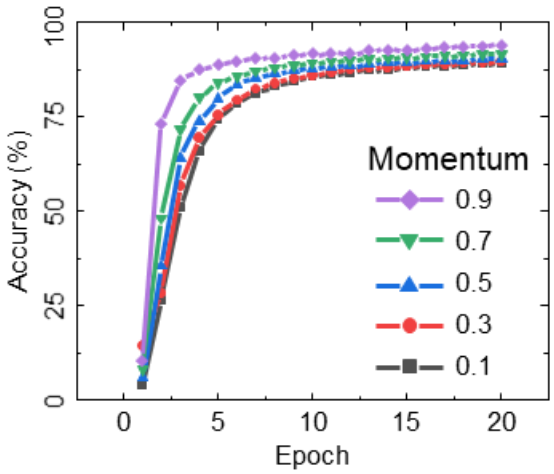

Figure S10 Recognition accuracy as a function of training epoch for different learning momentum values in the MNIST simulation.

Figure S11

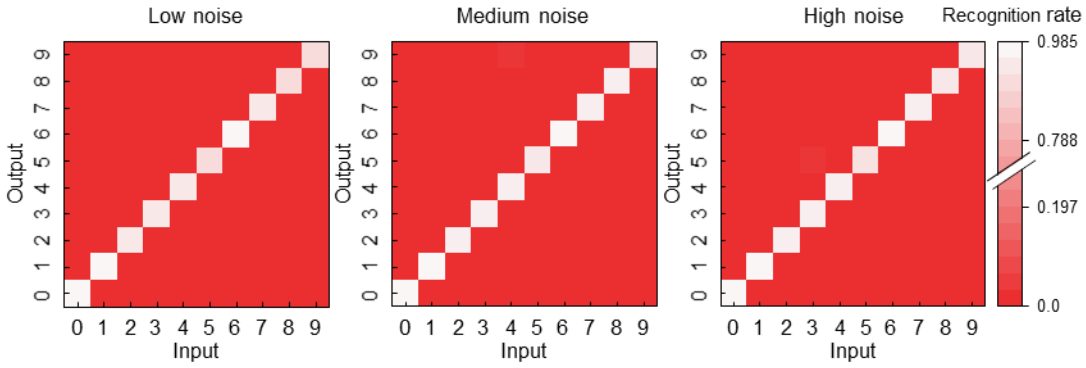

Figure S11. Confusion matrices for noisy samples.

Table S3. MNIST recognition tests raw data for high noise image

	input 0	input 1	input 2	input 3	input 4	input 5	input 6	input 7	input 8	input 9
Output 0	963	0	9	2	1	8	11	2	8	11
Output 1	0	1111	3	0	2	3	3	7	5	6
Output 2	2	3	956	18	5	2	4	24	6	1
Output 3	2	2	14	953	1	36	1	5	25	11
Output 4	0	0	9	0	926	6	10	6	10	30
Output 5	4	2	0	9	0	790	11	1	18	6
Output 6	6	4	9	2	12	15	915	0	12	1
Output 7	2	2	12	14	2	6	2	968	12	23
Output 8	1	11	16	9	3	18	1	2	874	4
Output 9	0	0	4	3	30	8	0	13	4	916
Total test	980	1135	1032	1010	982	892	958	1028	974	1009

Supplementary Note 1

Calculation of electron doping concentration using the parallel-plate capacitor model

For graphene transferred onto SiO_2, assuming the oxide layer as a parallel plate capacitor while neglecting the quantum capacitance, the carrier concentration can be calculated as:

$$\Delta \boldsymbol{n} = \boldsymbol{n} - \boldsymbol{n}_{\mathbf{i}} = \Delta \boldsymbol{Q}/\boldsymbol{e} = \boldsymbol{C}\frac{\Delta \boldsymbol{V}_{\mathbf{CNP}}}{\boldsymbol{ed}} = \frac{\boldsymbol{\varepsilon}_{\mathbf{SiO_2}}}{\boldsymbol{ed}}|\boldsymbol{V}_{\mathbf{G}} - \boldsymbol{V}_{\mathbf{dirac}}|$$

Here, Q is the charge density, C is the capacitance per area, and d = 300 nm is the thickness of the SiO_2 substrate. If we assume the carrier concentration at Dirac point ($\boldsymbol{n_i}$) to be zero, then:

$$\boldsymbol{n} \sim \Delta \boldsymbol{n} = \frac{\boldsymbol{\varepsilon}_{\mathbf{SiO_2}}}{\boldsymbol{ed}}|\boldsymbol{V}_{\mathbf{G}} - \boldsymbol{V}_{\mathbf{dirac}}|$$

The Fermi energy can be calculated using a step function approximation. By substituting the density of states of graphene into the Fermi-Dirac distribution function and simplifying, we can obtain:

$$\boldsymbol{n} \sim \frac{\mathbf{2}}{\boldsymbol{\pi}}\frac{\mathbf{1}}{(\hbar \boldsymbol{v}_{\mathbf{F}})^2}\int_{\boldsymbol{E}_{\mathbf{F}}}^{\mathbf{0}}|\boldsymbol{E}|\boldsymbol{dE} = \frac{\mathbf{2}}{\boldsymbol{\pi}}\frac{\mathbf{1}}{(\hbar \boldsymbol{v}_{\mathbf{F}})^2}\frac{\mathbf{1}}{\mathbf{2}}\boldsymbol{E}_{\mathbf{F}}^{\mathbf{2}} = \frac{\mathbf{1}}{\boldsymbol{\pi}}\frac{\mathbf{1}}{(\hbar \boldsymbol{v}_{\mathbf{F}})^2}\boldsymbol{E}_{\mathbf{F}}^{\mathbf{2}}$$

By rearranging the equation in terms of the Fermi energy $\boldsymbol{E}_{\mathbf{F}}$, we derive

$$\boldsymbol{E}_{\mathbf{F}} = \hbar \boldsymbol{v}_{\mathbf{F}}\sqrt{\boldsymbol{\pi p}} = \hbar \boldsymbol{v}_{\mathbf{F}}\sqrt{\boldsymbol{\pi}\frac{\boldsymbol{\epsilon}_{\mathbf{SiO_2}}}{\boldsymbol{ed}}|\boldsymbol{V}_{\mathbf{G}} - \boldsymbol{V}_{\mathbf{dirac}}|}$$

Here, $\hbar$ is reduced Planck constant and $\boldsymbol{v}_{\mathbf{F}}$ is fermi velocity.

In Figure 3c, the energy barrier between graphene and ZnO is determined by subtracting the Fermi energy shift induced by electrostatic gating from the Schottky barrier. The Fermi energy corresponding to each gate voltage was obtained by substituting the gate voltage into the above equation.

Supplementary Note 2

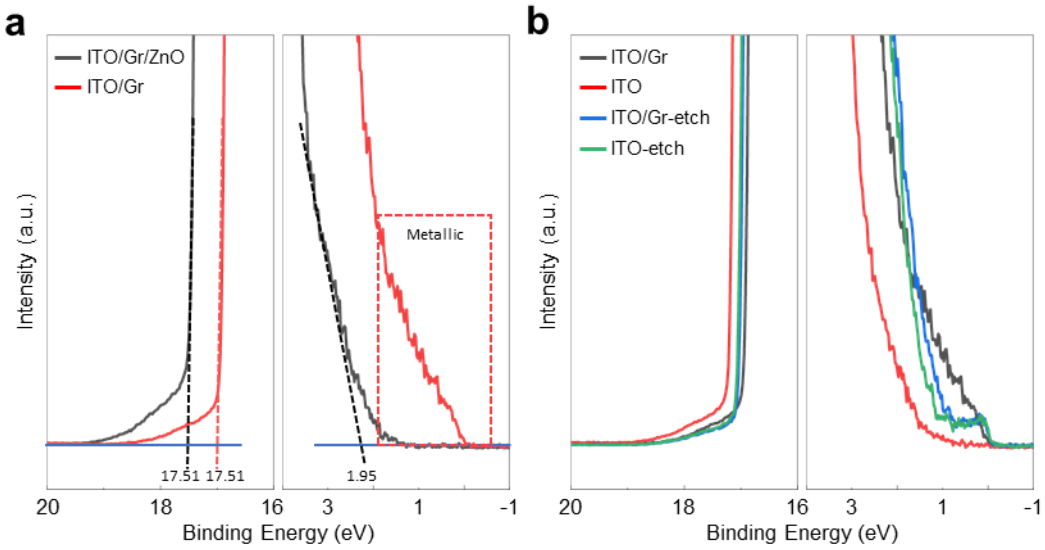

Figure S12. a. UPS spectra of Gr and GZO on ITO substrate. **b**. UPS spectra of Gr and Gr-etch.

Due to the monolayer graphene's thickness, which is much thinner than the conventional UV penetration depth (on the nanometer scale), there exists a possibility that the measured spectrum may include contributions from the indium tin oxide (ITO) substrate beneath the graphene. To validate this, comparative UPS measurements were conducted on the ITO/Gr heterostructure before and after an etching process to remove the graphene layer. The UPS spectrum of ITO/Gr was found to differ from that of bare ITO, confirming that the measured photoelectrons originate from the graphene layer. Furthermore, after the graphene was etched away, the UPS spectrum of the ITO/Gr sample matched that of bare ITO, as shown in ITO/Gr-etch and ITO-etch spectra in Figure S12b. This supports the conclusion that the UPS spectrum of ITO/Gr represents photoemission from graphene itself and not from the underlying ITO substrate.

[1] S. Lei, F. Wen, B. Li, Q. Wang, Y. Huang, Y. Gong, Y. He, P. Dong, J. Bellah, A. George, L. Ge, J. Lou, N. J. Halas, R. Vajtai, P. M. Ajayan, *Nano Lett.* **2015**, *15*, 259.
[2] J. Lee, S. Pak, Y.-W. Lee, Y. Cho, J. Hong, P. Giraud, H. S. Shin, S. M. Morris, J. I. Sohn, S. Cha, J. M. Kim, *Nat. Commun.* **2017**, *8*, 14734.
[3] G. S. Syed, Y. Zhou, J. Warner, H. Bhaskaran, *Nat. Nanotechnol.* **2023**, *18*, 1036.
[4] G. Wu, X. Zhang, G. Feng, J. Wang, K. Zhou, J. Zeng, D. Dong, F. Zhu, C. Yang, X. Zhao, D. Gong, M. Zhang, B. Tian, C. Duan, Q. Liu, J. Wang, J. Chu, M. Liu, *Nat. Mater.* **2023**, *22*, 1499.
[5] G.-X. Zhang, Z.-C. Zhang, X.-D. Chen, L. Kang, Y. Li, F.-D. Wang, L. Shi, K. Shi, Z.-B. Liu, J.-G. Tian, T.-B. Lu, J. Zhang, *Sci. Adv.* **2023**, *9*, eadi5104.
[6] P. Xie, Y. Xu, J. Wang, D. Li, Y. Zhang, Z. Zeng, B. Gao, Q. Quan, B. Li, Y. Meng, W. Wang, Y. Li, Y. Yan, Y. Shen, J. Sun, J. C. Ho, *Nat. Commun.* **2024**, *15*, 8298.
[7] Z. Wang, M. Li, H. Yang, S. Shao, J. Li, M. Deng, K. Kang, Y. Fang, H. Wang, J. Zhao, *ACS Nano* **2024**, *18*, 14298.
[8] Y. Wang, S. Nie, S. Liu, Y. Hu, J. Fu, J. Ming, J. Liu, Y. Li, X. He, L. Wang, W. Li, M. Yi, H. Ling, L. Xie, W. Huang, *Adv. Mater.* **n.d.**, *n/a*, 2404160.
[9] F. Su, J. Wan, D. Wang, *Adv. Funct. Mater.* **n.d.**, *n/a*, 2425627.
[10] S. Ge, F. Huang, J. He, Z. Xu, Z. Sun, X. Han, C. Wang, L.-B. Huang, C. Pan, *Adv. Opt. Mater.* **2022**, *10*, 2200409.
[11] Y. Li, Y. Zhang, Y. Wang, J. Sun, Q. You, M. Zhu, L. Li, T. Deng, *Adv. Funct. Mater.* **2024**, *34*, 2302288.
[12] Y. Qian, J. Li, J. Shen, Y. Ke, S. Yu, W. Li, X. Xu, H. Ling, W. Huang, M. Yi, *Adv. Electron. Mater.* **2023**, *9*, 2300135.